Acta Crystallographica Section F
Structural Biology and Crystallization Communications
ISSN 1744-3091

Structure of a 6-pyruvoyltetrahydropterin synthase homolog from *Streptomyces coelicolor*

James E. Spoonamore,[a] Sue A. Roberts,[a] Annie Heroux[b] and Vahe Bandarian[a,c]*

[a]Departments of Biochemistry and Molecular Biophysics, University of Arizona, Tucson, AZ 85721, USA, [b]Biology Department, Brookhaven National Laboratory, Upton, NY 11973, USA, and [c]Department of Chemistry, University of Arizona, Tucson, AZ 85721, USA

Correspondence e-mail: vahe@email.arizona.edu

Received 24 June 2008
Accepted 21 August 2008

PDB Reference: 6-pyruvoyltetrahydropterin synthase homolog, 3d7j, r3d7jsf.

The X-ray crystal structure of the 6-pyruvoyltetrahydropterin synthase (PTPS) homolog from *Streptomyces coelicolor*, SCO 6650, was solved at 1.5 Å resolution. SCO 6650 forms a hexameric T-fold that closely resembles other PTPS proteins. The biological activity of SCO 6650 is unknown, but it lacks both a required active-site zinc metal ion and the essential catalytic triad and does not catalyze the PTPS reaction. However, SCO 6650 maintains active-site residues consistent with binding a pterin-like substrate.

1. Introduction

Biopterin is an essential cofactor in mammalian nitric oxide synthase and aromatic hydroxylation reactions, but is not commonly found in bacteria. Glycosylated biopterin analogs are synthesized by a number of photosynthetic bacteria and may be involved in photoreception or UV protection (Wachi *et al.*, 1995; Yamazawa *et al.*, 1999). Tetrahydrobiopterin (BH_4) is biosynthesized in three steps from GTP by the successive actions of GTP cyclohydrolase I (GCH I), 6-pyruvoyltetrahydrobiopterin synthase (PTPS) and sepiapterin reductase (SR). PTPS is a zinc-containing protein that catalyzes two successive Amadori rearrangements to convert 7,8-dihydroneopterin triphosphate to 6-pyruvoyltetrahydropterin.

The hexameric rat PTPS assumes a 'tunnel' fold (T-fold; Nar *et al.*, 1994; PDB code 1b66), which has also been reported for GTP cyclohydrolase I (GCH I; Nar *et al.*, 1995; PDB code 1gtp), dihydroneopterin aldolase/epimerase (DHN aldolase; Sanders *et al.*, 2004; PDB code 1rrw) and urate oxidase (Retailleau *et al.*, 2004; PDB code 1r51). The T-fold of PTPS contains a dimer of trimers that form a stacked toroid. The active site of PTPS lies at the interface of three subunits (*A*, *A*′ and *B*; Ploom *et al.*, 1999; see gray residues in Fig. 1). Three histidine imidazole side chains from subunit *A* (His23, His48 and His50) and the hydroxyl group at C2′ of the substrate coordinate an essential divalent zinc metal ion in the active site. An Asp88-His89 duo from subunit *B* activates Cys42 of subunit *A* to initiate the catalytic cycle (see Fig. 1). The endocyclic nitrogen at N3 and the exocyclic amino group at C2 hydrogen bond to the side-chain carboxylate of Glu107, while the backbone amide of the preceding residue (Thr106) hydrogen bonds to the pyrimidine carbonyl O atom (at C3). Additionally, a second glutamic acid side chain from subunit *A* (Glu133) forms a hydrogen bond to the C1′ hydroxyl of the substrate (Fig. 1). While subunit *A*′ is not directly involved in catalysis, it lines one side of the active site and the backbone carbonyl of Met70 forms a hydrogen bond to the exocyclic amino group, presumably stabilizing the bound substrate.

The genome sequence of *Streptomyces coelicolor* (Bentley *et al.*, 2002) revealed the presence of a PTPS homolog (SCO 6650), which is nestled in a cluster of genes that appears to be conserved in all strains of actinomyces sequenced to date. In addition to PTPS, this cluster also contains a GTP cyclohydrolase II homolog, SCO 6655, which we have shown to catalyze the conversion of GTP to 2-amino-5-formylamino-6-ribosylamino-4(3*H*)-pyrimidinone 5′-phosphate (FAPy; Spoon-

amore *et al.*, 2006). A biological imperative for the co-localization of these genes is not clear.

As part of a program to assign the biological function of this cluster, SCO 6650 was cloned, overexpressed in *Escherichia coli* and purified as either His_6-tagged or native protein. Both the native and His_6-tagged proteins crystallized readily and the structure of the selenomethionine-substituted His_6-tagged protein was solved to 1.5 Å resolution. The model reveals that SCO 6650 lacks nearly all the catalytically essential residues but retains the residues required for binding a pterin-like substrate.

2. Materials and methods

2.1. Materials

Restriction endonucleases were from New England Biolabs. Expression vectors pET28a and pET29a and expression strain *E. coli* BL21 (DE3) were from Novagen. The pGEM-T Easy kit was from Promega. LB refers to Lennox Broth. *Pfu* Turbo and DH5α were from Invitrogen. Purification resins were obtained from GE Healthcare. All other chemicals were obtained from VWR Scientific and Sigma–Aldrich.

2.2. Protein expression and purification

The gene encoding the *S. coelicolor* PTPS homolog (*sco6650*) was amplified with Primer 1 (5′-GGAATTCCCATGGCATATGTTCAGCATCACCGTCCGCGATCAC-3′) and Primer 2 (5′-TTTTAAGCTTATTACAGCGCACGCTCGTAACTCGC-3′) from *S. coelicolor* genomic DNA and subcloned into the pGEM T-Easy vector prior to cloning into the *Nde*I/*Hin*dIII site of pET28a and pET29a overexpression plasmids for the expression of His_6 or native protein, respectively. The sequence of the final construct revealed that a nonconservative mutation had inadvertently been introduced (*via* Primer 2) during initial cloning. To correct this error, the gene was amplified from the cloning vector using Primer 1 and Primer 3 (5′-GCAAGCTTATTACAGCGCACGCTCGTAACTCGCCCAGGC-3′) and recloned into the expression vectors. DNA sequencing confirmed that the error had been corrected.

Native protein was prepared by transformation of *E. coli* BL21 (DE3) with the pET29 expression vector bearing SCO 6650. Transformants were grown overnight in LB containing 34 µg ml^{-1} kanamycin prior to the inoculation of large-scale (1 l) growth containing 34 µg ml^{-1} kanamycin. Expression was induced by the addition of 0.1 m*M* isopropyl β-D-1-thiogalactopyranoside at an $OD_{600\,nm}$ of ∼1; cells were harvested after 4 h. For purification, cell pastes were resuspended into 25 ml 0.02 *M* Tris–HCl pH 8 containing 0.5 m*M* DTT and supplemented with one tablet of Complete EDTA-free protease inhibitor (Roche). Cells were lysed by sonication and then centrifuged to remove cellular debris. The cleared lysate was applied onto a Q-Sepharose Fast Flow column (2.5 × 14.5 cm) that had been equilibrated with 0.02 *M* Tris–HCl pH 8 containing 0.5 m*M* DTT; the protein was eluted with a linear gradient of 0–0.5 *M* KCl in the loading buffer; SCO 6650 eluted at ∼0.25 *M* KCl. Fractions that contained SCO 6650, as determined by SDS–PAGE, were pooled. Pooled fractions were dialyzed against 4 l 0.02 *M* Tris–HCl pH 8.0 containing 0.5 m*M* DTT with one buffer change. SCO 6650 was concentrated with a 10 000 Da molecular-weight cutoff centrifugal concentrator (YM-10 membrane, Amicon) and flash-frozen in liquid nitrogen until needed. Protein stock was quantified using the BCA protein-assay kit (Pierce) with BSA as a standard.

Selenomethionine-labeled N-terminally His_6-tagged protein was expressed in M9 minimal media supplemented with selenomethionine as described previously (Doublié, 1997). The protein was purified essentially as described for the native protein above, except that an additional gel-filtration step was included as follows. Dialyzed and concentrated Q-Sepharose fractions were applied onto a Sephacryl S-300 column (2.6 × 60 cm) equilibrated with 0.02 *M* Tris–HCl pH 8 containing 0.5 m*M* DTT. The protein was eluted with the same buffer.

Metal analysis of the selenomethionine-labeled protein by ICP-OES (Garratt–Callahan) revealed 2.1 equivalents of selenium in each monomer, which is consistent with the post-translational removal of the N-terminal methionine, resulting in the presence of two Se atoms in each monomer.

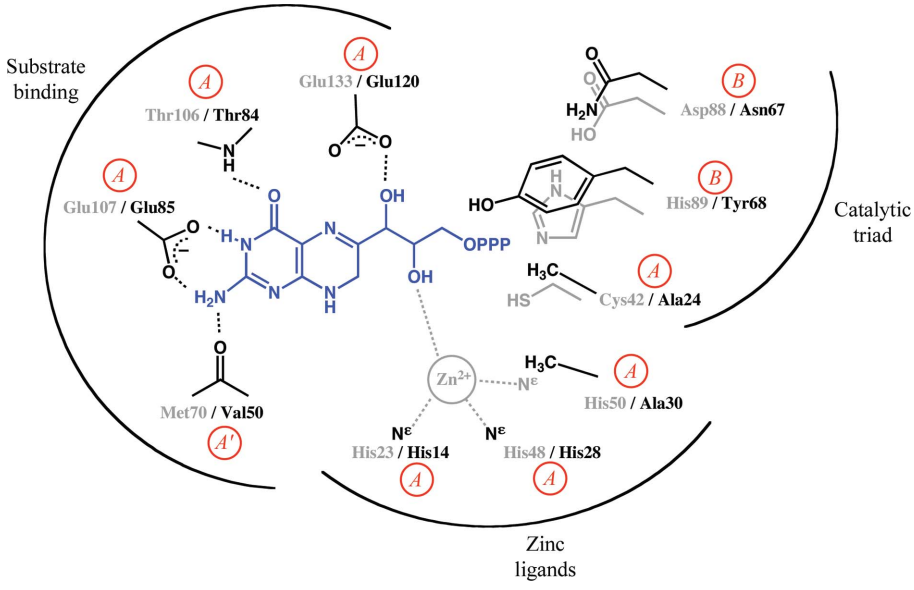

Figure 1
Summary of interactions between *Rattus rattus* PTPS and its substrate, 7,8-dihydroneopterin triphosphate (PDB code 1b66). The active site is composed of residues from three adjacent subunits (*A*, *A*′ and *B*). For each residue, the contributing subunit is indicated in red. Residues from the rat PTPS structure are in gray and the corresponding residues in SCO 6650 are shown in black. The residues that bind the pterin in rat PTPS (Glu133, Thr106, Val107 and Met70) are identical to those in SCO 6650.

Table 1
Data-collection, phasing and refinement statistics.

Values in parentheses are for the outermost shell.

	SeMet crystal 1			
	Peak	Remote	Inflection	SeMet crystal 2
Crystal class, space group	Orthorhombic, $P2_12_12_1$	Orthorhombic, $P2_12_12_1$	Orthorhombic, $P2_12_12_1$	
Unit-cell parameters (Å)	a = 77.5, b = 87.8, c = 120.9	a = 77.5, b = 87.8, c = 120.9	a = 77.5, b = 87.8, c = 120.9	a = 77.4, b = 88.0, c = 120.9
Z (molecules per ASU)	6	6	6	
Temperature (K)	100	100	100	
Wavelength (Å)	0.9777	0.9600	0.9787	0.9771
Resolution (Å)	1.7	1.68	1.7	1.45
Total/unique reflections	523224/165708	545914/175003	518212/165212	958738/140447
Completeness (%)	96 (71)	97 (78)	96 (77)	96 (72)
Mean $I/\sigma(I)$	34 (2.3)	36 (2.3)	37 (2.5)	44 (2.2)
$R_{\rm merge}$†	0.08 (0.49)	0.08 (0.50)	0.08 (0.45)	0.12 (0.49)
FOM (solve)	0.60 at 2.6 Å			
$R_{\rm cryst}/R_{\rm free}$‡				0.206/0.224
R.m.s.d. bonds (Å)				0.010
R.m.s.d. angles (°)				1.2
Ramachandran plot, residues in				
Most favorable regions (%)				92.5
Additional allowed regions (%)				7.5
Average B (Å^2)				20.1

† $R_{\rm merge} = \sum_{hkl}\sum_i |I_i(hkl) - \langle I(hkl)\rangle| / \sum_{hkl}\sum_i I_i(hkl)$, where $\langle I(hkl)\rangle$ is the mean intensity of all symmetry-related reflections $I_i(hkl)$. ‡ $R_{\rm cryst} = (\sum |F_{\rm obs} - F_{\rm calc}|)/\sum F_{\rm obs}$. $R_{\rm free}$ as for $R_{\rm cryst}$ but using a random subset of the data (5%) not included in the refinement.

2.3. Crystallization and structure solution

Conditions yielding crystals of SeMet-containing His_6-SCO 6650 were found using the sparse-matrix screening kits Crystal Screen I and II from Hampton Research. The hanging-drop method was utilized in these experiments. The SeMet histidine-tagged SCO 6650 was crystallized as follows: a 3 µl aliquot of the protein solution, which typically contained 40 mg ml^{-1} protein in 0.02 *M* Tris–HCl pH 8.0 and 0.5 m*M* DTT, was combined with 3 µl of a solution containing 2 *M* NaCl and 10% PEG 6000. The well volume was 0.5 ml. Crystals grew at room temperature in 7 d and were flash-frozen using 3.2 *M* NaCl, 10% PEG 6000 for cryoprotection.

Selenium MAD data were collected at 100 K using an ADSC Quantum-4 CCD detector on beamline X26C at Brookhaven National Laboratory. Data were collected at three wavelengths (see Table 1 for statistics) and reduced using *HKL*-2000 (Otwinowski & Minor, 1997). Data to 2.6 Å resolution were used for phasing. Nine selenium positions were located and initial phases were calculated using *SOLVE* (Terwilliger & Berendzen, 1999). Density modification,

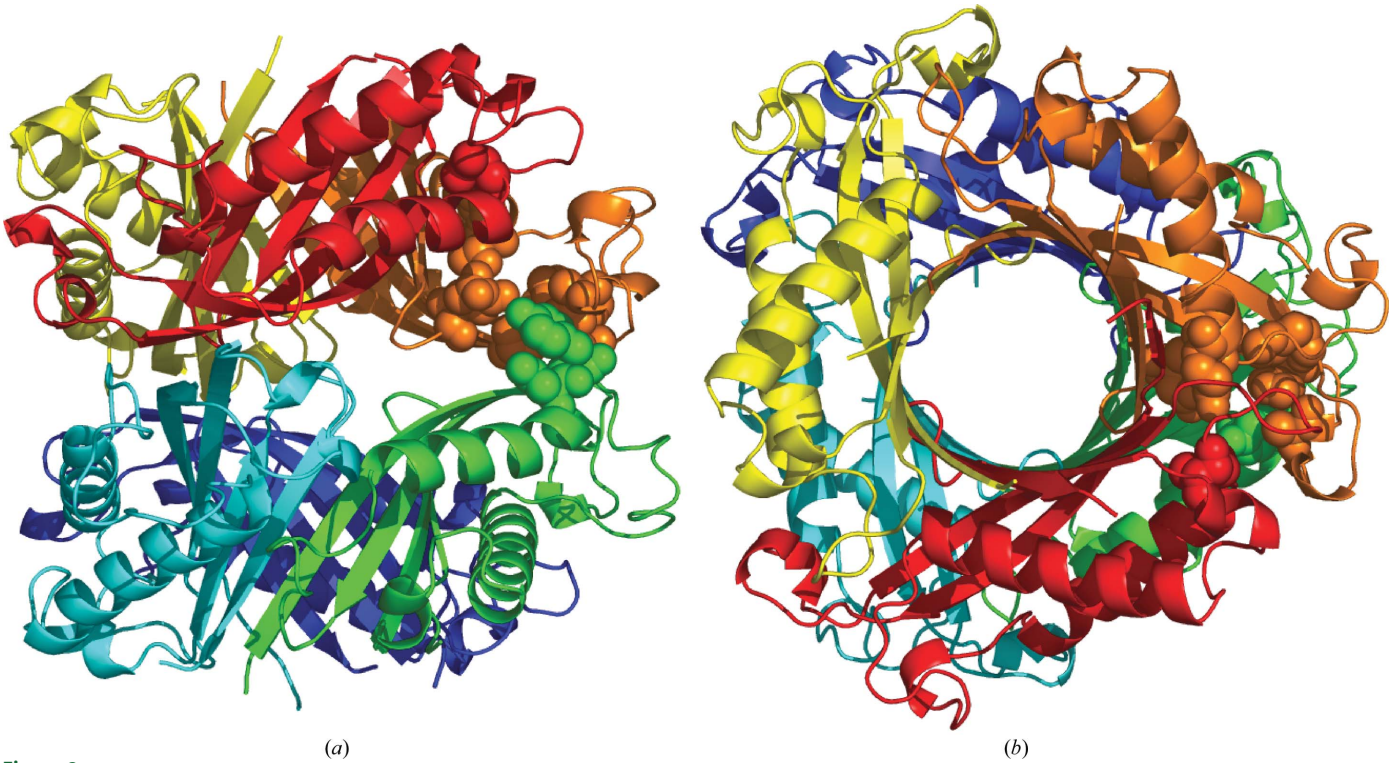

(*a*) (*b*)

Figure 2
The X-ray crystal structure of SCO 6650. The SCO 6650 hexamer observed across and down the T-fold barrel. Spheres represent residues highlighted in Fig. 1, demonstrating that three subunits contribute to the active site of the PTPS. The structural drawings were generated with *PyMOL* (DeLano, 2002).

phase extension to 1.5 Å resolution and initial structure building were performed using *RESOLVE* (Terwilliger, 2003). The structure was refined using *REFMAC*5 (Murshudov *et al.*, 1997) and rebuilt with *Coot* (Emsley & Cowtan, 2004). There is residual difference electron density on the faces and the empty center of the hexamer along the pseudo-threefold axis. Disc-shaped pieces of electron density, presumably from partially occupied histidine residues of the His_6 tag (sequence MGSSHHHHHHSSGLVPRGSH), can be seen stacked on Trp25 residues from each chain located at the top and bottom of the central cavity. Except for these partially occupied stacked histidine residues, the residual electron density could not be interpreted and since neither the residue number nor chain identification of these histidine residues could be determined, they were not included in the model.

3. Results and discussion

3.1. Overall structure of SCO 6650 and comparison to PTPS homologs

Structurally, SCO 6650 is a member of the T-fold protein family, which also includes GTP cyclohydrolase I, dihydroneopterin aldolase and urate oxidase (Murzin *et al.*, 1995). The asymmetric unit of the His_6-tagged protein crystals contains a hexamer, which is likely to be the biologically relevant oligomerization state of the protein. Gel-filtration studies with the native SCO 6650 are consistent with the presence of a hexamer (data not shown). The protein is composed of two stacked trimers. A 12-stranded antiparallel β-barrel forms the central tunnel in the protein; the overall diameter of the trimer is 55 Å (Fig. 2) and the hexamer is 53 Å in length.

The X-ray crystal structures of several PTPS homologs have been reported (Nar *et al.*, 1994; Ploom *et al.*, 1999) or deposited in the Protein Data Bank (PDB codes 1y13, 2g64, 2a0s, 2dtt, 2dj6 and 2oba). The crystallization of the *E. coli* homolog (YgcM) was reported recently (Seo *et al.*, 2008). With the exceptions of the *Pyrococcus horikoshii* and *E. coli* PTPS homologs, which are trimers, PTPS proteins are hexamers. Site-directed mutagenesis studies have confirmed that the active site of PTPS has contributions from both toroids (A, A' and B in Fig. 2), suggesting a hexameric biological unit (Bürgisser *et al.*, 1994, 1995; Ploom *et al.*, 1999). The trimeric PTPS homologs lack several key catalytic residues (Cys42, Asp88 and His89; see Fig. 2) which would be contributed by a subunit from an adjacent toroid (subunit B in Fig. 2). However, we note that Asp88 and His89 are conserved in both the *Py. horikoshii* and *E. coli* sequences.

Structural similarities between SCO 6650 and *Py. horikoshii* (PDB code 2dtt), *Pseudomonas aeruginosa* (2oba), *Rattus rattus* (1b66), *Plasmodium vivax* (2a0s) or *Pl. falciparum* (1y13) PTPS homologs were confirmed by structural overlays. Interestingly, despite low sequence identities (15–21%) and similarities (29–40%), the root-mean-squared deviation of C^{α} atoms varies between 1.6 and 2.1 Å for the oligomers or 1.3 and 1.6 Å for the monomers (Krissinel *et al.*, 2004).

3.2. Comparison of SCO 6650 to PTPS proteins

A multiple sequence alignment comparing the PTPS sequences from *R. rattus*, *Ps. aeruginosa* and *Py. horikoshii* with that of SCO 6650 is shown in Fig. 3. In each case, an X-ray crystal structure of the protein is available, allowing the locations and roles of conserved residues to be evaluated. While the alignment reveals substantial sequence similarities, several residues that are known to be required for the action of PTPS are absent from SCO 6650 (see Fig. 1).

While the putative active-site cleft in SCO 6650 is similar to that described for PTPS (Ploom *et al.*, 1999), the residues that line the site are different. In the following discussion, we utilize the *R. rattus* X-ray crystal structure (PDB code 1b66) for comparison to SCO 6650, since significant biochemical data highlight the importance of various residues in the active site of the protein (Bürgisser *et al.*, 1995; see Fig. 1 for schematic comparison). The *R. rattus* PTPS structure shows that a zinc divalent metal ion is bound to the imidazole side chains of three His residues (23, 48 and 50) as well as the 2′-OH of the substrate. The zinc-coordinating residues are required for activity (Bürgisser *et al.*, 1995). In SCO 6650, an Ala residue is found at position 30. A His→Leu site-directed variant at the corresponding position in rat PTPS (His50) loses the ability to bind the zinc ion and is catalytically inactive. Zinc is not observed in the crystal structure of SCO 6650, nor could it be detected by ICP-OES analysis of protein

```
                                       Zn                          Cat        Zn
Py. horikoshii   ----MKSRIIVRTSFDAA H -----------AVKVGDH W ED--V H G H TFFLEVAIEGEIK-
Ps. aeruginosa   -------ELFKEFTFESA H RLP--------HVPEGHK C GR--L H G H SFRVAIHIEGEVDP
R. rattus        VGLRRRARLSRLVSFSAS H RLHSPSLSAEENLKVFGK C NNPNG H G H NYKVVVTIHGEIDP
SCO 6650         -----MFSITVRDHIMIA H SFRG---------DVFGP A QR--L H G A TFLVDATFRREQLD
                        :     :  : *                           * *   .: :    :. *

                      Sub               Cat                Sub
Py. horikoshii   -NGYV M DFLELRKIVEE-ITKEL DH RNLN-NI--FEN--PT TE NIALWIGERIRDKLPP-
Ps. aeruginosa   HTGWI R DFAEIKAIFKP-IYEQL DH NYLN-DIPGLEN--PT SE NLCRWIWQQLKPLLP--
R. rattus        VTGMV M NLTDLKEYMEEAIMKPL DH KNLDLDVPYFADVVST TE NVAVYIWENLQRLLPV-
SCO 6650         EDNIV V DIGLATQELGA-VVGAL NY RNLD-NEPDFAGVNTS TE FLAKVIADRLAERVHKG
                   . : :   :     .   :    * :: . *: :   : .  .: :*  :.  * :.:   :

                                    Sub
Py. horikoshii   -------YVKLKRVVLW E GKDNGVELEW--
Ps. aeruginosa   ---------ELSKVRVH E TCTSGCEYRGD-
R. rattus        -------G-ALYKVKVY E TDNNIVVYKGE-
SCO 6650         ALGEGARGLAGLTVTLH E SHVAWASYERAL
                                 * :  *          .
```

Figure 3

A multiple sequence alignment of PTPS homologs from *Py. horikoshii* (gi:14590525), *Ps. aeruginosa* (gi:126031480), *R. rattus* (gi:4929886) and SCO 6650 generated with *ClustalW* (Thompson *et al.*, 1994). The boxes in the alignment highlight the positions of the zinc-liganding histidine residues (Zn), the catalytic triad (Cat) and the substrate-binding residues (Sub) in PTPS.

preparations, even when the growth medium was supplemented with 0.1 m*M* $ZnSO_4$ (data not shown). A trio of residues in the active site of PTPS, Cys42, His89 and Asp88, are thought to be involved in initiating catalysis. In SCO 6650, the Cys42–His89–Asp88 triad is replaced by Ala24–Tyr68–Asn67. Collectively, the substitutions that are apparent in SCO 6650 relative to rat PTPS (summarized in Fig. 1), where biochemical studies have confirmed the importance of these residues, suggest that SCO 6650 cannot catalyze the conversion of 7,8-dihydroneopterin triphosphate to 6-pyruvoyltetrahydropterin (Bürgisser *et al.*, 1995). In fact, we have been unable to detect this activity with SCO 6650 under conditions where the mouse PTPS is active (data not shown).

While the catalytic residues required for PTPS function are not conserved in SCO 6650, the residues involved in binding of a pyrimidine-containing substrate are retained. In this analysis, ligand-bound models of PTPS from *Py. horikoshii* (Bagautdinov *et al.*, 2007; PDB code 2dtt), *R. rattus* (Ploom *et al.*, 1999; PDB code 1b66), *Pl. vivax* (PDB 2a0s) and *Pl. faciparum* (PDB code 1y13) were utilized. Each of these proteins has a Ser/Thr-Glu motif (Thr106-Glu107 in rat PTPS) that hydrogen bonds to the pyrimidine ring. In the available substrate-bound PTPS structures, the carboxylate side chain of the glutamate residue (Glu107 of rat PTPS) hydrogen bonds the exocyclic amino group at C2 and the endocyclic N3 nitrogen. The backbone amide of the Ser/Thr residue (Thr106 of rat PTPS) hydrogen bonds to the carbonyl O atom at C4. A similar duo of residues (Thr84-Glu85, see Fig. 1) are observed in an analogous position in the SCO 6650 structure. A backbone carbonyl (Met70 in rat PTPS) also hydrogen bonds to the exocyclic amino group. The backbone carbonyl of Val50 in SCO 6650 appears to be in the same position as the backbone carbonyl of Met70. Furthermore, the carboxylate side chain of Glu133, which has a catalytic role in rat PTPS (Bürgisser *et al.*, 1995), interacts with the 1′-OH group of the substrate; Glu120 of SCO 6650 is in the same position. Therefore, in contrast to the catalytic triad and zinc ion-binding site, there is striking conservation in SCO 6650 of the residues that interact with the substrate, suggesting that it utilizes a substrate that is structurally similar to 7,8-dihydroneopterin triphosphate (see Fig. 1 for summary of interactions). We should note that a similar constellation of residues (corresponding to Thr84-Glu85) has been noted in the T-fold proteins GCH I and DHN aldolase (Hennig *et al.*, 1998) for binding of the pyrimidine ring of the substrate.

The authors wish to thank Annie Dahlgran for cloning *sco6650* and purifying some of the preparations used in this work. Reid McCarty and Alberto Rascon are acknowledged for gifts of mouse PTPS and *E. coli* GCH I, respectively. Data were measured on beamline X26C of the National Synchrotron Light Source (NSLS). Financial support for NSLS comes principally from the Offices of Biological and Environmental Research and of Basic Energy Sciences of the US Department of Energy and from the National Center for Research Resources of the National Institutes of Health. VB acknowledges support from the National Institutes of Health (GM072623). JES was partially supported by an NIH predoctoral training grant (GM08804). In addition, the research of VB was supported (in part) by a Career Award in Biomedical Sciences from the Burroughs Wellcome Fund.

References

Bagautdinov, B., Sugahara, M. & Kunishima, N. (2007). *Acta Cryst.* F**63**, 15–17.
Bentley, S. D. *et al.* (2002). *Nature (London)*, **417**, 141–147.
Bürgisser, D. M., Thöny, B., Redweik, U., Hess, D., Heizmann, C. W., Huber, R. & Nar, H. (1995). *J. Mol. Biol.* **253**, 358–369.
Bürgisser, D. M., Thöny, B., Redweik, U., Hunziker, P., Heizmann, C. W. & Blau, N. (1994). *Eur. J. Biochem.* **219**, 497–502.
DeLano, W. L. (2002). *The PyMOL Molecular Graphics System.* DeLano Scientific, San Carlos, California, USA.
Doublié, S. (1997). *Methods Enzymol.* **276**, 523–530.
Emsley, P. & Cowtan, K. (2004). *Acta Cryst.* D**60**, 2126–2132.
Hennig, M., D'Arcy, A., Hampele, I. C., Page, M. G., Oefner, C. & Dale, G. E. (1998). *Nature Struct. Biol.* **5**, 357–362.
Krissinel, E. & Henrick, K. (2004). *Acta Cryst.* D**60**, 2256–2268.
Murshudov, G. N., Vagin, A. A. & Dodson, E. J. (1997). *Acta Cryst.* D**53**, 240–255.
Murzin, A. G., Brenner, S. E., Hubbart, T. & Chothia, C. (1995). *J. Mol. Biol.* **247**, 536–540.
Nar, H., Huber, R., Heizmann, C. W., Thöny, B. & Bürgisser, D. (1994). *EMBO J.* **13**, 1255–1262.
Nar, H., Huber, R., Meining, W., Schmid, C., Weinkauf, S. & Bacher, A. (1995). *Structure*, **3**, 459–466.
Otwinowski, Z. & Minor, W. (1997). *Methods Enzymol.* **276**, 307–326.
Ploom, T., Thöny, B., Yim, J., Lee, S., Nar, H., Leimbacher, W., Richardson, J., Huber, R. & Auerbach, G. (1999). *J. Mol. Biol.* **286**, 851–860.
Retailleau, P., Colloc'h, N., Vivarès, D., Bonneté, F., Castro, B., El Hajji, M., Mornon, J.-P., Monard, G. & Prangé, T. (2004). *Acta Cryst.* D**60**, 453–462.
Sanders, W. J. *et al.* (2004). *J. Med. Chem.* **47**, 1709–1718.
Seo, K. H., Supangat, Kim, H. L., Park, Y. S., Jeon, C. O. & Lee, K. H. (2008). *Acta Cryst.* F**64**, 105–107.
Spoonamore, J. E., Dahlgran, A. L., Jacobsen, N. E. & Bandarian, V. (2006). *Biochemistry*, **45**, 12144–12155.
Terwilliger, T. C. (2003). *Acta Cryst.* D**59**, 38–44.
Terwilliger, T. C. & Berendzen, J. (1999). *Acta Cryst.* D**55**, 849–861.
Thompson, J. D., Higgins, D. G. & Gibson, T. J. (1994). *Nucleic Acids Res.* **22**, 4673- 4680.
Wachi, Y., Burgess, J. G., Iwamoto, K., Yamada, N., Nakamura, N. & Matsunaga, T. (1995). *Biochim. Biophys. Acta*, **1244**, 165–168.
Yamazawa, A., Takeyama, H., Takeda, D. & Matsunaga, T. (1999). *Microbiology*, **145**, 949–954.